Applied Radiation and Isotopes 173 (2021) 109703

Contents lists available at ScienceDirect

Applied Radiation and Isotopes

journal homepage: http://www.elsevier.com/locate/apradiso

A novel monitoring method for gamma irradiation facility based on radio-voltaic and photovoltaic effects

Mingxin Bian [a], Xiaobin Tang [a,b,*], Zhiheng Xu [a], Zhenfeng Hou [a], Zicheng Yuan [a], Kai Liu [a]

[a] Department of Nuclear Science and Technology, Nanjing University of Aeronautics and Astronautics, 29 Yudao St., Nanjing, 210016, China
[b] Key Laboratory of Nuclear Technology Application and Radiation Protection in Astronautics (Nanjing University of Aeronautics and Astronautics), Ministry of Industry and Information Technology, 29 Yudao St., Nanjing, 210016, China

ARTICLE INFO

Keywords:
Co-60 frame
Radio-voltaic
Photovoltaic
Electrical signal curve
Cherenkov photon

ABSTRACT

This paper presents a novel monitoring method for gamma irradiation facility, which has the advantages of big view, accurate and working in event of a power outage. The state of radioactive source is monitored based on the property of electrical signal curves from photovoltaic devices when they are facing the source frame, and these electrical signals are generated by radio-voltaic and photovoltaic effects. GaAs based photovoltaic device was selected as the module to convert the rays near the radioactive source into electrical signals by the two above effects, and a Co-60 facility for irradiation processing was used as monitored object in this work. The influence of parameters such as the distance between the Co-60 frame and the photovoltaic device array, better electrical signals for forming curves on the monitoring effect were analyzed by Geant4. And the monitoring effect of the Co-60 frame in many cases was studied by Geant4 and experiment. Simulation results show that there are optimal parameters to achieve best monitoring effect, and the distribution of the Co-60 rods on the frame, the working condition and integrity of the Co-60 frame can be clearly reflected with this method. The consistency of the tendency of the electrical signal curves in verification experiment and Geant4 simulation verified the feasibility of this monitoring method. This method may provide new ideas for monitoring system designed for irradiation facility, nuclear power plants and other scenarios with rays.

1. Introduction

In recent years, with the exploration of irradiation technology, it has attracted more and more attention due to its special advantages of pollution-free, simple operation and low energy consumption. Its application field has been expanded to food preservation, nuclide production, material modification, etc (Choi et al., 2009; M'Garrech and Ncib, 2009; Shagufta, 2007). The Co-60, Cs-137 and other radionuclides as well as the neutron beam in the reactor are usually used for irradiation processing due to the rays with extreme penetrability they produced. In the operation design of irradiation facility, the radionuclides such as Co-60 are usually encapsulated in many cylindrical rods, and they are fixed horizontally on a multi-row frame, which are called Co-60 rod and Co-60 frame respectively. And the irradiation process is performed in a concrete-made irradiation chamber. When the equipment of the irradiation facility is being repaired or replaced, the Co-60 frame will be placed in a 7 m-deep well, which located in the irradiation chamber to shield γ rays to ensure the safety of the workers (Yusof et al., 2007; Mohammed et al., 2017). It is essential to monitor the position and integrity of the Co-60 frame due to the risk from the γ rays (Kim et al., 2017; Kellett and Bersillon, 2017). In the current application, there is usually a dosimeter fixed in the irradiation chamber, and it can judge roughly the position of the Co-60 frame (in irradiation chamber or well) according to its reading. Sometimes, a camera is attached to the well wall for real-time monitoring (Fig. 1(a)) (Schöppner et al., 2012; Baeza et al., 2017). However, the reading of dosimeter cannot accurately reflect the position of the Co-60 frame, and it cannot monitor the situation of few Co-60 rods falling from the frame to the floor of the irradiation chamber, which would bring the radiation risk to the staffs when they enter the irradiation chamber and the Co-60 frame was placed in the well. The limited view of camera makes it impossible to monitor the whole ascent and descent process of the Co-60 frame, and it cannot be used when a power outage occurs. What's worse, the image quality will gradually decline with the service time due to the color center effect in

* Corresponding author. Key Laboratory of Nuclear Technology Application and Radiation Protection in Astronautics (Nanjing University of Aeronautics and Astronautics), Ministry of Industry and Information Technology, 29 Yudao St., Nanjing, 210016, China.
E-mail address: tangxiaobin@nuaa.edu.cn (X. Tang).

https://doi.org/10.1016/j.apradiso.2021.109703
Received 29 October 2020; Received in revised form 26 February 2021; Accepted 22 March 2021
Available online 26 March 2021

camera glass and the radiation degradation of the electronic devices inside it, which also cannot accurately monitor the integrity of the Co-60 frame (Wirtenson and White, 1997; Cho et al., 2014).

Based on the previous research about the application of Cherenkov light, detection of radiant particles and conversion of radiant energy, this paper proposes a monitoring method based on "radio-voltaic/photovoltaic effects" for gamma irradiation facility (Shu et al., 2018; Zhang et al., 2019; Guo et al., 2019). There are at least three types of particles, namely, the γ rays produced by the decay of radioactive nuclei, the electrons generated by the interaction of γ rays with water molecules, and the Cherenkov photons generated by the propagation of high-speed electrons in water, exist in the well (Huang et al., 2009). And when photon is incident into the photovoltaic (PV) device, a current will appear in the external circuit due to the "photovoltaic effect". Similarly, γ rays and electrons have an analogous effect, which is called the "radio-voltaic effect". In this radiation environment, an array composed of multiple rows of PV devices is placed facing the radioactive source, and the position and activity information of the source frame can be reflected by the properties of curves between the electrical signals of each PV device and their lateral position. The electrical signal curves would change dynamically when the source frame is ascending or descending. When the frame was broken or some source rods dropped, the curves would change suddenly so it can attract the attention of the staff and take some corresponding measures.

In this work, a gamma irradiation facility with a Co-60 frame (Fig. 1 (a)) inside was used as the object to verify this monitoring method based on "radio-voltaic/photovoltaic effects". The influence of parameters in this method such as the distance between the Co-60 frame and the photovoltaic device array, better electrical signals for forming curves on the monitoring effect were analyzed by Geant4. And all cases of the Co-60 frame including uniformity, process of ascending and descending and some Co-60 rods dropped were simulated by Geant4. The results show that the state of Co-60 frame can be reflected clearly by the characteristics of electrical signal curves. A verification experiment confirmed that the Co-60 frame can be monitored accurately by this method. The effectiveness of this newly method for monitoring radioactive sources was verified by Geant4 simulation and experiment.

2. Material and method

2.1. Co-60 frame and PV device array

The Co-60 frame from the Radiation Center in Nanjing University of Aeronautics and Astronautics was used as the monitored object in Geant4 simulation and verification experiment. Its size and design are shown in Fig. 2.

The length and height of the frame are 2.5 m and 2.3 m respectively. It can be divided into four rows from top to bottom, and Y1 – Y4 indicate the number of different rows. There are 120 vacancies in every row, and each can load a Co-60 rod. The spacing between adjacent vacancies is approximately 0.7 cm. The Co-60 rod is a cylinder with a diameter of 1.1 cm and a height of 45.1 cm. The height difference between two adjacent rows of Co-60 rods is 55 cm. Each Co-60 rod in Fig. 2 has the same size and shape, while the different colors only represent different activities. In practical applications, the activity and arrangement of the Co-60 rods on the frame are different and uneven, which is for the need of replacement and replenishment and to ensure that all goods receive same dose. It is very meaningful that the uneven arrangement of the Co-60 rods can test the monitoring effect of this method on the uneven source frame.

A board with the same size of the Co-60 frame was used to load a GaAs based PV device array, that is, four rows of PV devices were fixed laterally on the surface. In this array, the number of rows of PV devices is consistent with Co-60 rods in the frame, and the height difference of the adjacent rows is same with the Co-60 frame as shown in Fig. 3(a). These PV devices were connected to the monitor in the control room. In the Geant4 simulation program, there are 4 rows of PV devices in the array corresponding to the 4 rows of Co-60 rods in the frame, while in the verification experiment, only two rows of PV devices in right half of Y1 and Y2 rows due to the symmetrical arrangement of Co-60 rods in the frame. The design of GaAs based PV device array in the Geant4 simulation and verification experiments are shown in Fig. 3(b) and (c) respectively, and the size of the PV device is 1 cm × 1 cm in both. In Geant4 simulation program, there are 220 PV devices in each row, because the vacancies at the left and right ends of each row in the frame are 2.2 m apart. In the verification experiment, there are 16 PV devices with 5 cm apart in Y1 and Y2 rows respectively due to the symmetrical arrangement rule of the Co-60 rods and the economics of the experiment. So they are in the range of X = 115 to X = 190 as shown in Fig. 3 (c).

2.2. Modeling and theoretical calculation method

The Geant4 was used to simulate the whole physical process of three particles, including the generation of γ rays, electrons and Cherenkov photons and the propagation of them in the well, as well as they incident into the GaAs based PV device. The main modules of the Geant4 program and their corresponding functions are shown in Fig. S1 in Supplementary Material. The energy of electrons and γ rays deposited in GaAs based PV device and the spectrum of Cherenkov photons incident on the surface of the PV device are calculated by the Geant4 program, which are used to calculate the electrical signal generated in the GaAs based PV device. The Geant4 program in the current work is derived from our team's previous research published in (Shu et al., 2018).

The electrical signals (including short circuit current density J_{sc}, open-circuit voltage V_{oc}, and maximum output power density P_{max}) generated in GaAs based PV device through the radio-voltaic and photovoltaic effects of the three particles were calculated according to

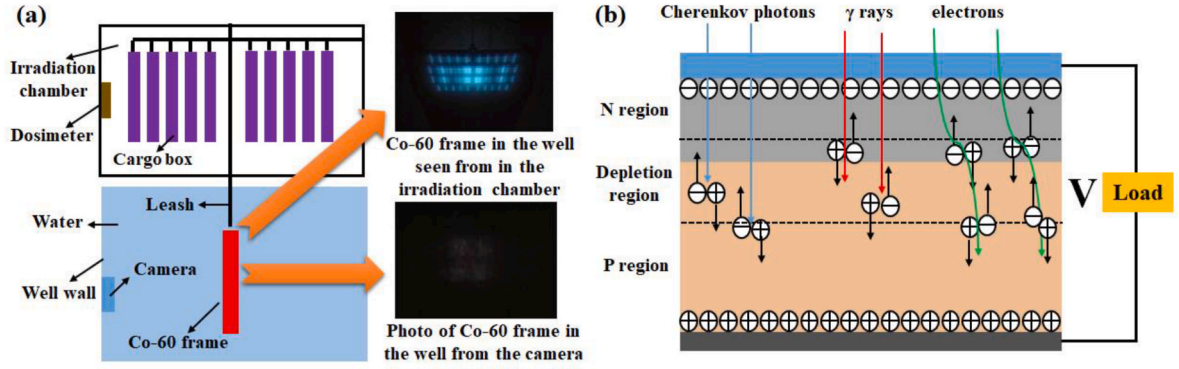

Fig. 1. a) Schematic of some components in the irradiation chamber. **b)** Schematic of radio-voltaic and photovoltaic effects.

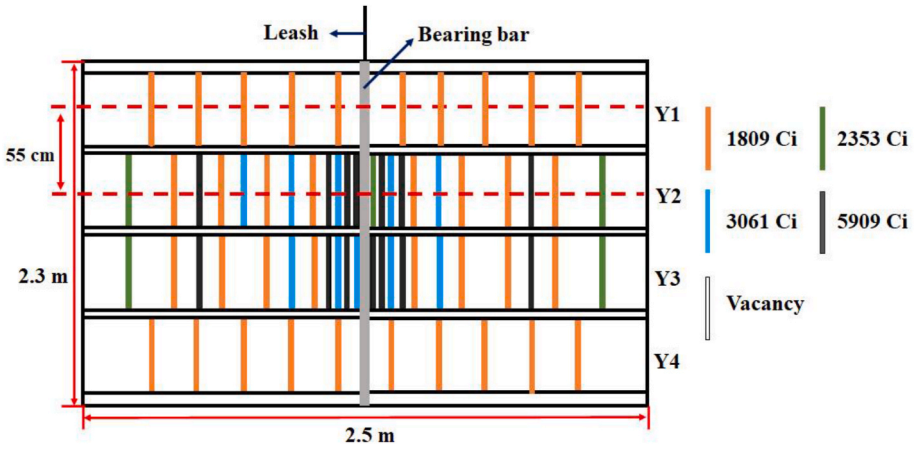

Fig. 2. Schematic of the Co-60 frame.

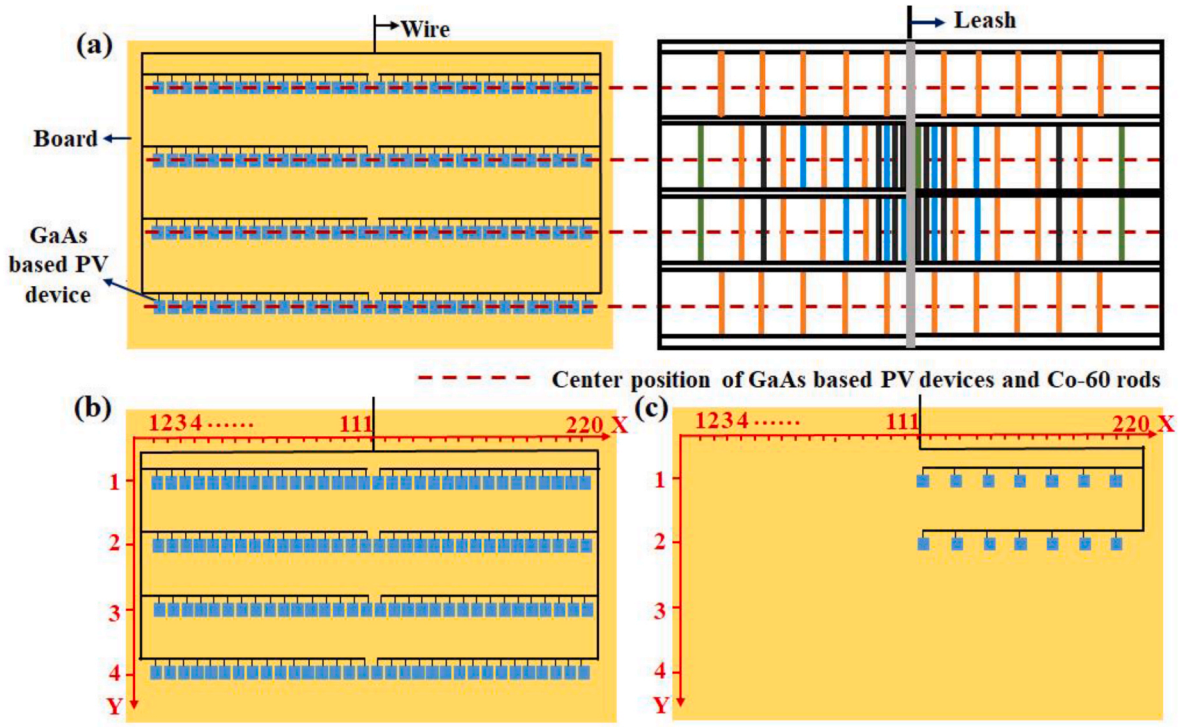

Fig. 3. a) Schematic of the PV device array in this monitoring method. PV device array in **b)** Geant4 simulation and **c)** verification experiment.

the following empirical formula.

The current density can be described by (Nelson, 2003):

$$J(V) = J_{sc} - J_0\left[exp\left(\frac{qV}{k_B T_a}\right) - 1\right] \tag{1}$$

where J_o represents the reverse saturation current density, k_B represents the Boltzmann constant, and T_a represents the water temperature in the well of 300 K. The J_{sc} is composed of $J_{sc}(RV)$ generated by the radio-voltaic effect and $J_{sc}(PV)$ generated by the photovoltaic effect, as shown as (Guo et al., 2018):

$$J_{sc} = J_{sc}(RV) + J_{sc}(PV) \tag{2}$$

In the radio-voltaic effect, the γ rays and the electrons interact directly with the GaAs based PV device to convert kinetic energy to electric energy. So the electrical output is related to the energy deposited inside the PV device. In calculation, the energy of γ rays and electrons deposited inside the GaAs based PV device is considered in generating electron-hole pairs (Gao et al., 2012). $J_{sc}(RV)$ can be expressed as:

$$J_{sc}(RV) = \frac{qE}{E_{ehp}} \tag{3}$$

$$E_{ehp} = 2.8E_g + 0.5 \tag{4}$$

where E represents the energy of γ rays and electrons deposited in the PV device, which was taken from the result of Geant4 program. E_{ehp} represents the energy required to generate an electron-hole pair, and E_g represents the bandgap of the GaAs of 1.43 eV. Equation (4) comes from Klein formula, and there will be some errors in the calculation of wide bandgap semiconductor materials. Therefore, it will cause a certain relative error in the calculation results (Sellin and Vaitkus, n.d.; Chang et al., 2014).

In the photovoltaic effect, Cherenkov photons were incident on the PV device to convert the light energy into electrical energy. $J_{sc}(PV)$

generated by Cherenkov photons can be represented by (Fthenakis, 2001):

$$J_{sc}(PV) = q\int_{E_g}^{\infty} b_s(E, T_a)dE \tag{5}$$

where $b_s(E, T_a)$ denotes the spectral density of Cherenkov photons incident on the PV device surface, which can be extracted from the EventAction module in the Geant4 program. In particular, the charge collection efficiency is set to 100% in both photovoltaic and radiovoltaic effects.

According to the Shockley equation, V_{oc} generated by the two effects can be expressed as:

$$V_{oc} = \frac{k_B T_a}{q} ln\left(\frac{J_{sc}}{J_0} + 1\right) \tag{6}$$

$$J_0 = q\int_{E_g}^{\infty} \frac{2F_a E^2}{h^3 c^2 [exp(E/k_B T_a) - 1]} dE \tag{7}$$

where h is the Planck constant, c is the photon velocity in a vacuum, F_a is the environmental geometrical factor equal to π (Tang et al., 2012).

The maximum output power density P_{max} is expressed by:

$$P_{max} = J_{sc} V_{oc} FF \tag{8}$$

where FF called the fill factor and its value can be calculated as (Tang et al., 2012):

$$FF = \frac{v_{oc} - ln(v_{oc} + 0.72)}{v_{oc} + 1} \tag{9}$$

where v_{oc} is the normalized open-circuit voltage equal to the ratio of V_{oc} to kT/q.

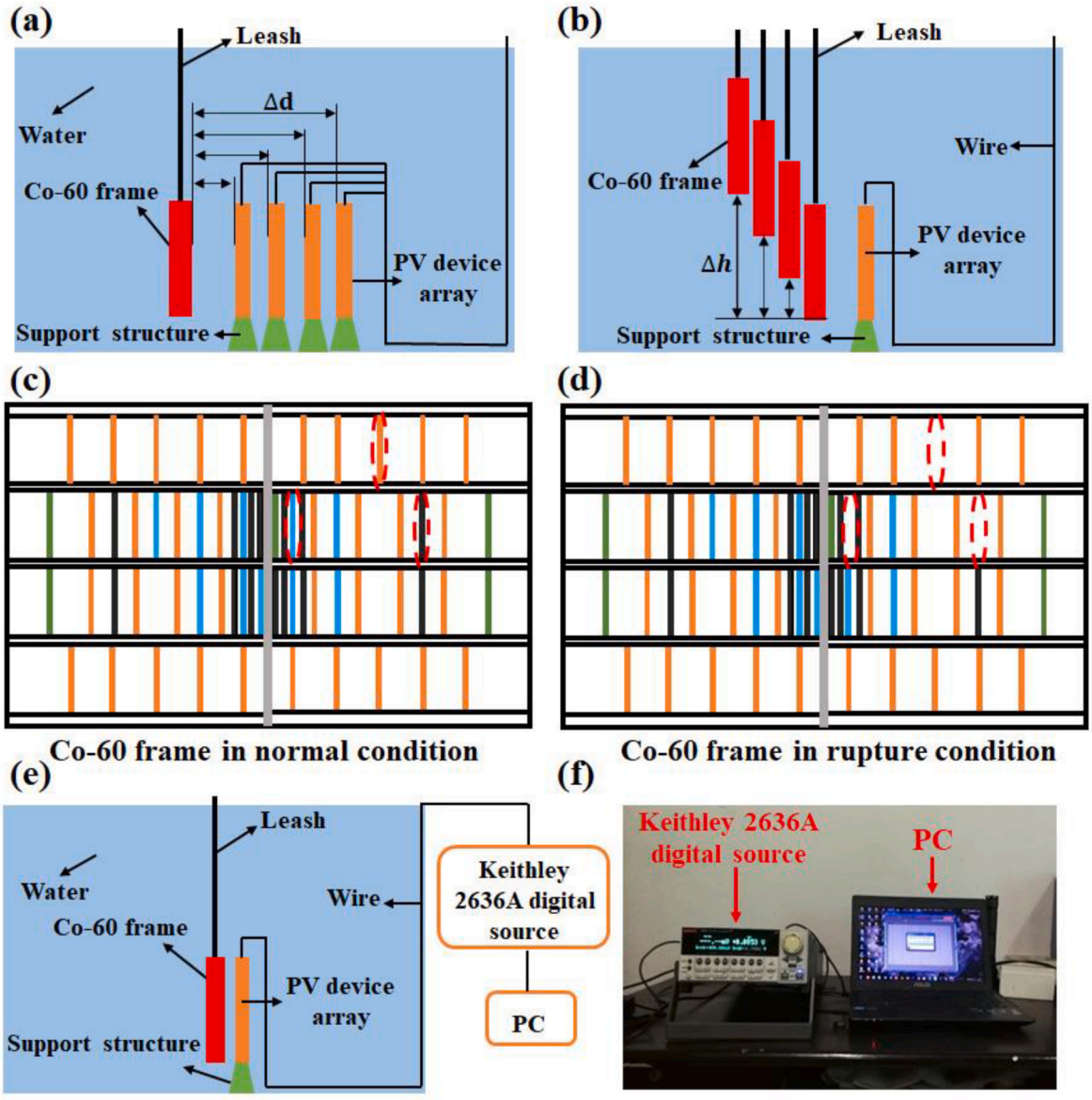

Fig. 4. a) Schematic of different distances from the Co-60 frame to the PV device array. **b)** Schematic of the Co-60 frame in the process of rise and fall. Comparison of Co-60 frame in **c)** normal and **d)** rupture conditions. **e), f)** Test schematic of verification experiment.

2.3. Application verification

In Geant4 simulation, the variation trend between the volatility of the electrical signal curves with its lateral position and the distance Δd from Co-60 frame to the PV device array was analyzed, and the curves that can reflect clearly the arrangement of Co-60 rods on the frame has the best electrical signal and distance. The best distance Δd and electrical signal will be applied in subsequent studies. The real-time monitoring effect was studied through the dynamic changes of the electrical signal curves during the rise and fall of the Co-60 frame, and the changes in the electrical signal curves were also explored when the Co-60 frame was ruptured and some Co-60 rods dropped. The schematic of the different distances from the Co-60 frame to the PV device array and the process of rise and fall of the Co-60 frame are shown in Fig. 4(a) and (b). The position of the Co-60 rods dropped in the frame is shown in Fig. 4(c). The feasibility of this method can be used to monitor radioactive source was verified through the Geant4 simulation for the above three conditions.

In the verification experiment, a polyethylene plastic board was used to load the PV device array. The reaction cross-section between polyethylene plastic and γ ray is very small (Hine and Brownell, 2013; Hu et al., 2020), which can reduce the generation of secondary electrons and scattered photons. This can reduce the impact of the polyethylene board on the electrical signal curves. The *I–V* characteristic of each PV device was tested by a digital source which was placed in a control room connected to the PV device with wires (Fig. 4(f)).

3. Simulation results and analysis

3.1. Influence of Δd and electrical signal on monitoring effect

The monitoring effect of this method is strongly affected by the distance Δd from the Co-60 frame to the PV device array and the electrical signals of the monitor. The distance range that can make the curves between the electrical signal of the PV devices and their lateral position with great volatility is the best range, and that electrical signal is suitable for the monitor.

Fig. 5 shows the I_{sc} and V_{oc} curves from the PV device array when the Co-60 frame facing the PV device array with different distances in the well.

In Fig. 5, both I_{sc} and V_{oc} curves fluctuate with the lateral positions of the PV devices, and the I_{sc} curves is significantly, while V_{oc} is not. The information (activity, position) of the Co-60 rods in Y1 and Y4 rows, Y2 and Y3 rows have a certain similarity, respectively. Consequently, the I_{sc} curves of corresponding rows also have a certain similarity. There are ten Co-60 rods with the same activity and separation distance periodically arranged in Y1 and Y4 rows. Therefore, ten crests with the same height and spacing appear periodically in the I_{sc} curves, as shown in Fig. 5(a) and (d). The height and positions of crests in the I_{sc} curves indicate the activity and position of the Co-60 rods in corresponding row, respectively. Similarly, the symmetry in the arrangement of Co-60 rods on Y2 and Y3 rows is reflected clearly by the I_{sc} curves of Y2 and Y3 rows. In particular, there is a Co-60 rod near the bearing bar at right half of Y2 row and left half of Y3 row with lower activity than that one at symmetrical position (The Co-60 rod with green near the bearing bar at right half of Y2 row and the blue one near the bearing bar at left half of Y3 row as shown in Fig. 2). A crest with lower height thus exists at the

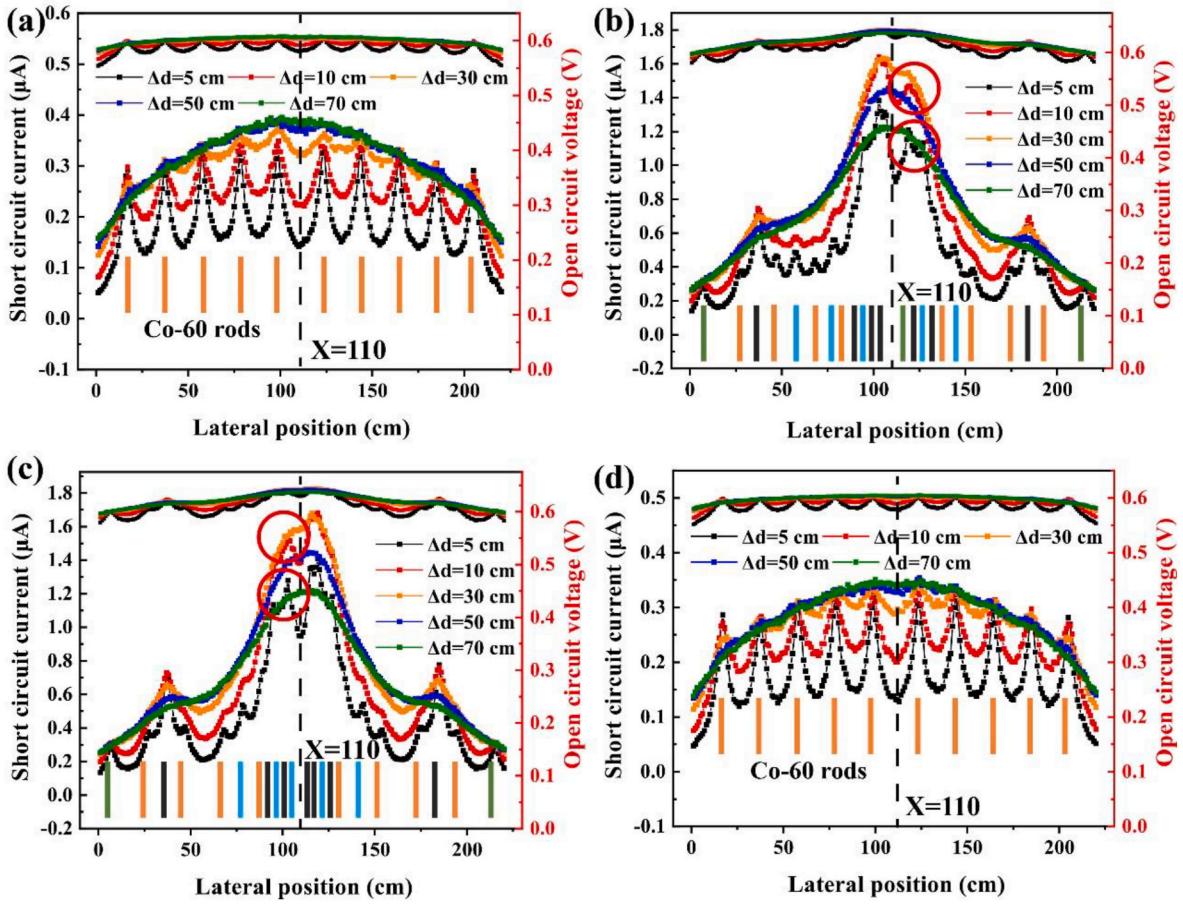

Fig. 5. I_{sc} and V_{oc} curves of the PV devices as a function of the distance from the array to the Co-60 frame in **a)** Y1 row, **b)** Y2 row, **c)** Y3 row, and **d)** Y4 row.

corresponding position in the I_{sc} curves of Y2 and Y3 rows, as indicated by the red circles in Fig. 5(b) and (c). However, the volatility of the I_{sc} curves of Y2 and Y3 rows is not as obvious as that of Y1 and Y4 rows, as shown in Fig. 5(b), (c) and Fig. 5(a), (d). This is limited by the spatial resolution ability of this monitoring method. There are many Co-60 rods with high activities densely arranged in Y2 and Y3 rows, and the adjacent spacing between them is less than that in Y1 and Y4 rows. Therefore, the volatility of the I_{sc} curves, which reflects the densely distributed Co-60 rods in Y2 and Y3 rows, is not very obvious. And the spatial resolution ability of this monitoring method may be related to the size of the PV devices, because the width of the PV devices is equal to the distance between adjacent points on the I_{sc} curves. This also means that more and smaller PV devices can be considered in each row to reduce the distance between adjacent points on the I_{sc} curves, making the I_{sc} curves finer and smoother. P_{max} curves with similar properties are shown in Fig. S2.

The volatility in I_{sc} curves changes with different distance Δd between the Co-60 frame and the PV device array as shown in Fig. 5. When Δd = 5 cm or 10 cm, I_{sc} fluctuate markedly with the PV devices' lateral position, and the activity and position of the Co-60 rods in frame could be monitored according to the properties of crest and trough in the I_{sc} curves. However, as the distance Δd increases, I_{sc} increases but the volatility in curves decreases until it disappears. The reason for this phenomenon maybe that the angle of absorption of Cherenkov photons, γ rays, and electrons by the PV device toward the Co-60 frame increases as Δd increases. Therefore, the increase in electrical signal is due to the increased number of the three particles received in the PV device. Nevertheless, the contribution of the special Co-60 rod facing a PV device in electrical signal is reduced, and the PV device cannot specifically receive the particles generated by that one.

In other words, there maybe an optimal range of the distance Δd between the Co-60 frame and the PV device array to achieve best monitoring effect due to the absorption angle of PV device. And the optimal range of the distance Δd is determined by the activity, size and type of radioactive source and the material of the PV device. In this Co-60 irradiation facility, the reasonable distance Δd that can form the electrical signal curves with great volatility was set to be 10 cm instead of smaller in order to avoid affecting the normal ascending and descending operation of the Co-60 frame. The maximum and minimum electrical signals of the PV device in each row when the Co-60 frame is 10 cm away from the PV device array are shown in Table 1. P_{max} of the PV devices is shown in Table S1. Table 1 shows that I_{sc} varies obviously with the lateral position of PV devices, while V_{oc} is not. Similarly, the variation in P_{max} is significant as shown in Table S1. In summary, for GaAs based PV device, I_{sc} and P_{max} can be used as important electrical signal indicators for monitor.

3.2. Real-time monitoring effect

The real-time monitoring effect of this method was analyzed when the Co-60 frame is in the process of ascent or descent, and the distance Δd between the Co-60 frame and the PV device array was set to 10 cm, I_{sc} and P_{max} were used as indicators for monitor. Only the rise process is analyzed since the fall is the inverse process. During the rise of the Co-60 frame, the change of the I_{sc} curves of four rows of PV devices is shown in Fig. 6.

As shown in Fig. 6, the I_{sc} curves from four rows show similar characteristic with the rise of the Co-60 frame, that is, they dynamically reflect the information of the Co-60 rods in a row which they were facing at that moment. However, the change of each I_{sc} curve is not exactly same because the height of each row of PV device is different. Taking the I_{sc} curve of Y1 row as an example, it shows the information of the Co-60 rods on from Y1 row to Y4 row orderly during the ascent of the Co-60 frame, because those PV devices in Y1 row at the highest position in array. While the I_{sc} curve of Y4 row come to 0 directly as the Co-60 frame rises due to the lowest position in array. In current work, the interval of rise distance of the Co-60 frame is set to 20 cm, and the detailed change in the I_{sc} curves with rise of the Co-60 frame is shown in Fig. S3. Similar characteristic in the P_{max} curves are shown in Fig. S4. In practical applications, the Co-60 frame can be monitored comprehensively by the changes of the four I_{sc} or P_{max} curves. If the I_{sc} and P_{max} in four curves are 0, it means that the Co-60 frame is completely lifted into the irradiation chamber above the well. This monitoring method can carry out real-time monitoring of the ascent and descent process of the Co-60 frame according to the changes in four electrical signals curves.

3.3. Monitoring effect under accident

Three Co-60 rods with representative activities and positions were selected for analyzing the monitoring ability of the method under an accident of the rupture of the Co-60 frame. They are at X = 165 in Y1 row with an activity of 1809 Ci, and X = 115, X = 185 in Y2 row with activities of 3061 and 5909 Ci respectively.

Fig. 7(c) shows that when a Co-60 rod in Y1 row dropped, the I_{sc} of several PV devices in the vicinity of the corresponding position in Y1 row suddenly decrease, and the corresponding crest in curve transform to trough; the best I_{sc} in curve decreases from 0.32 μA to 0.1 μA, and the relative change rate is approximately 70%. When the two Co-60 rods in Y2 row dropped, it can be seen that a crest in I_{sc} curve of Y2 row missing at X = 185, and I_{sc} of the some PV devices near X = 115 in Y2 row decreases considerably, resulting in a remarkable decrease in amplitude of the I_{sc} curve as shown in Fig. 7(e). When three Co-60 rods dropped, the I_{sc} of the PV devices at other positions in the array does not change, only the electrical signals of PV devices at the positions near the dropped Co-60 rods change significantly. And the similar characteristic in P_{max} curves are shown in Fig. S5. It can be concluded that this method can perform real-time and accurate monitoring when some Co-60 rods dropped.

From the above simulation work, it can be concluded that for different radioactive sources (activity, ray properties) and material of the PV device, there are optimal range for the distance Δd from the PV device array to the radioactive source and the best indicators for the monitor.

This method can accurately monitor the radioactive source in real time in all cases. The irradiation facility equipped with this method can further reduce or avoid the risk of staff due to entering the irradiation chamber by mistake, although camera and dosimeter have been used.

Table 1
Output results of PV devices in each row of the array.

Row	I_{sc}(max)/μA	I_{sc}(min)/μA	ΔI/μA	Relative change rate/%	V_{oc}(max)/V	V_{oc}(min)/V	ΔV_{oc}/V	Relative change rate/%
Y1	0.349	0.082	0.267	76.5	0.604	0.566	0.038	6.29
Y2	1.642	0.2	1.442	87.8	0.644	0.589	0.055	8.54
Y3	1.682	0.199	1.483	88.1	0.644	0.589	0.055	8.54
Y4	0.335	0.075	0.26	77.6	0.603	0.564	0.039	6.47

*The percentage relative change rate in current [I_{sc}(min)/I_{sc}(max)-1] × 100.
**The percentage relative change rate in voltage [V_{oc}(min)/V_{oc}(max)-1] × 100.

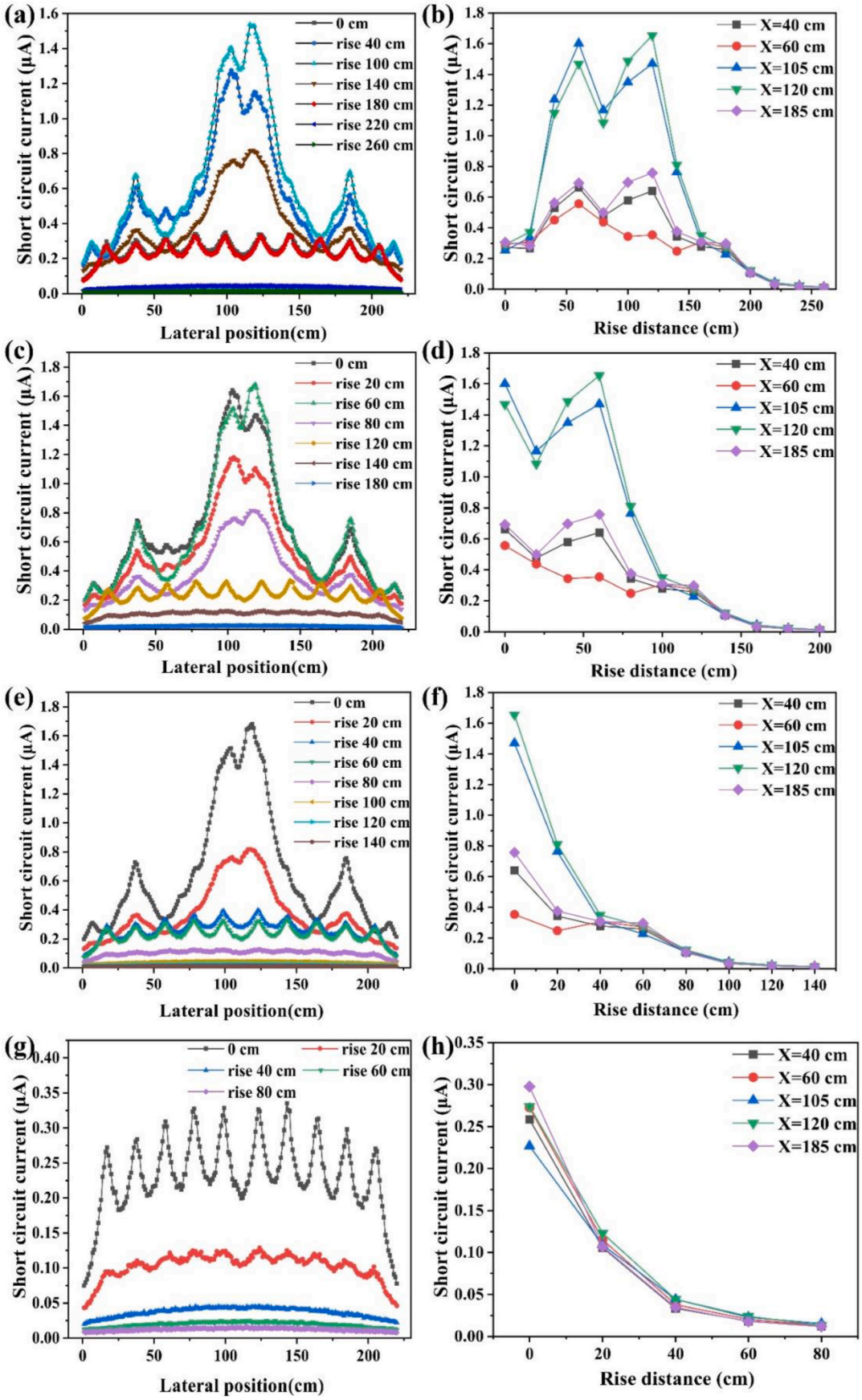

Fig. 6. Diagram of I_{sc} curves of **a)** Y1, **c)** Y2, **e)** Y3, **g)** Y4 row with rise distance of the Co-60 frame. I_{sc} of some PV devices at special positions in **b)** Y1, **d)** Y2, **f)** Y3, **h)** Y4 row with different rise distances of the Co-60 frame.

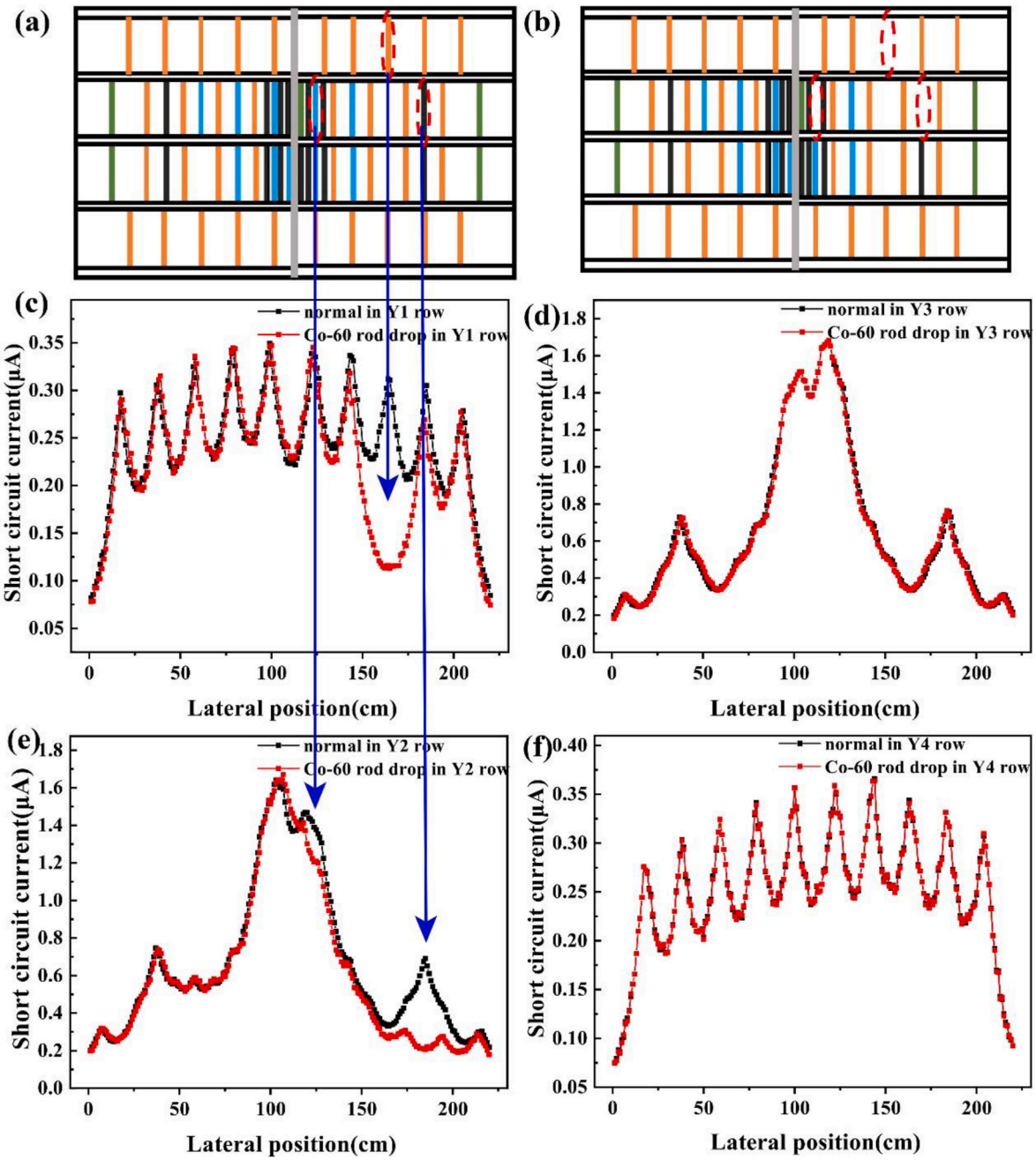

Fig. 7. Schematic of Co-60 frame in **a)** normal and **b)** rupture condition. Change in I_{sc} curve of **c)** Y1, **d)** Y3, **e)** Y2, **f)** Y4 row before and after the Co-60 rods dropped.

4. Experiment results and analysis

The Co-60 frame in the verification experiment is the same with simulation program, and the distance Δd between Co-60 frame and the GaAs based PV device array is about 10 cm. The comparison between the experimental and simulation results is shown in Fig. 8.

Fig. 8(a) and (b) depict the comparison of I_{sc} curves of right half of Y1 and Y2 rows in experimental and simulation results, respectively. For Y1 row, the I_{sc} curves in simulation and experimental results show the same variation trend at the same position. There are four crests with same height in both I_{sc} curves because of four Co-60 rods with the same activity in the frame. The positions of the crests in the I_{sc} curves were exactly correspond to the positions of the Co-60 rods in the frame as shown in Fig. 8(a). In Y2 row, the I_{sc} curves in both experimental and simulation results show the arrangement of Co-60 rod. In particular, a Co-60 rod with high activity at X = 185 is shown by a crest in I_{sc} curves. The similar comparison about the P_{max} curves in the experimental and simulation results is shown in Fig. S6.

The difference between simulation and experimental results can be attributed to the following reasons. In the experiment, some Cherenkov photons did not enter inside of the PV device due to the reflection on the surface. The electrical output will be reduced due to the defects in the PV device (Li et al., 2020). The electrical signal received by the digital source will also be reduced due to the attenuation occurred in the wire (Leo, 1994; Huang et al., 2017). On the other hand, the charge collection efficiency of the GaAs based PV device is not 100% in reality.

Although the differences between simulation and experimental results exist, the variation trend at the special positions indicate the information of the Co-60 rods is same. The consistency of the variation trend between simulation and experimental results verified the feasibility of this method for monitoring irradiation facility.

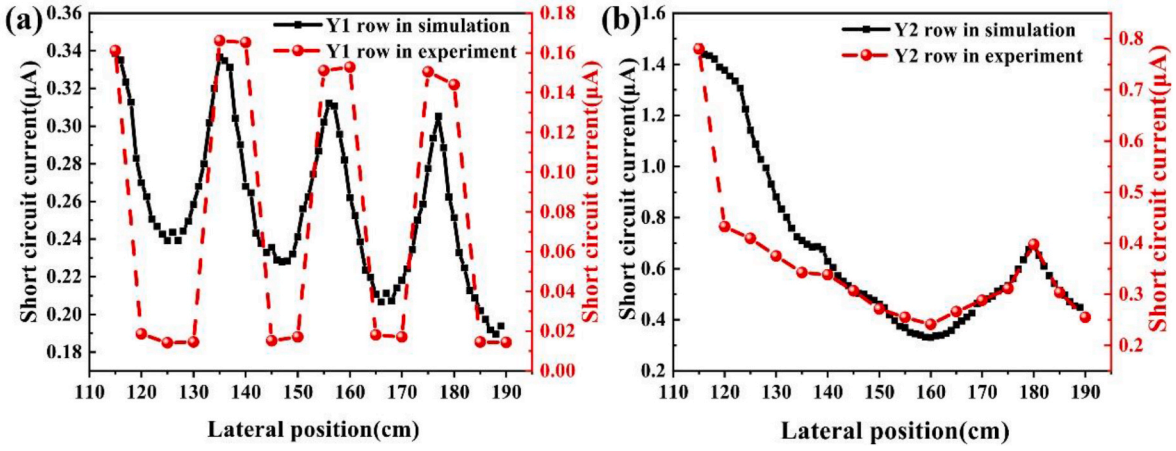

Fig. 8. Experimental and simulation results of I_{sc} of PV devices in **a)** Y1 and **b)** Y2 row.

5. Conclusion

A novel monitoring method based on "radio-voltaic/photovoltaic effects" for gamma irradiation facility was proposed and verified to compensate for the deficiency of the current monitoring method with camera and dosimeter. The conversion from the rays near the radioactive source to electrical signal with photovoltaic device is innovatively applied to this monitoring method. Based on Geant4 particle transport simulation and application verification in actual scenarios, this method has been found to be feasible and effective, and can meet actual monitoring needs.

According to the variation and amplitude of the electrical signal curves of the PV devices, the information about arrangement, position, activity and integrality of the Co-60 frame can be obtained. There is an optimal range for the distance Δd from the PV device array to the radioactive source and electrical signal for the monitor to achieve the best monitoring effect. In electrical signal curves, the relative change rate in the lateral direction exceeds 75%, and the huge volatility can reflect the Co-60 rods' information. When the Co-60 frame is in motion, the change of electrical signal curves can monitor it in real time. If some Co-60 rods dropped, the sudden change at specific positions on the curves can remind us in time and accurately find the position of the Co-60 rod. The consistency of variation trend in the experimental and simulation results verified the feasibility of the monitoring method.

This monitoring method with special principles has advantages of reliability, long life, big view and can work normally when a power outage occurs. It could replace or be combined with underwater camera and dosimeter to ensure the safety of an irradiation facility. Moreover, this method can provide new ideas for new generation monitoring systems applied to irradiation facilities, nuclear power plants and other scenarios with rays.

Funding

This work was supported by the National Natural Science Foundation of China (Grant Nos. 12005101 and 11675076), China Postdoctoral Science Foundation (Grant No. 2019M661836), the Fundamental Research Funds for the Central Universities (Grant No. NP2018462).

CRediT authorship contribution statement

Mingxin Bian: Conceptualization, Investigation, Software, Methodology, Writing. **Xiaobin Tang:** Investigation, Methodology, Validation. **Zhiheng Xu:** Validation, Review, Investigation. **Zhenfeng Hou:** Software, Methodology. **Zicheng Yuan:** Investigation, Validation, Supervision. **Kai Liu:** Investigation, Validation, Supervision.

Declaration of competing interest

The authors declare that they have no known competing financial interests or personal relationships that could have appeared to influence the work reported in this paper.

Appendix A. Supplementary data

Supplementary data to this article can be found online at https://doi.org/10.1016/j.apradiso.2021.109703.

References

Baeza, A., Corbacho, J.A., Caballero, J.M., Ontalba, M.A., Vasco, J., Valencia, D., 2017. Development of an advanced radioactive airborne particle monitoring system for use in early warning networks. J. Radiol. Prot. 37, 642.
Chang, Y., Chen, C., Liu, P., Zhang, J., 2014. A betavoltaic microcell based on Au/s-SWCNTs/Ti Schottky junction. Sensors Actuators A Phys 215, 17–21.
Cho, J.W., Choi, Y.S., Jeong, K.M., 2014. Monitoring performance of the cameras under the high dose-rate gamma ray environments. Health Phys. 106, S47–S58.
Choi, J., Kim, H.-J., Kim, J.-H., Byun, M.-W., Chun, B.S., Ahn, D.H., Hwang, Y.-J., Kim, D.-J., Kim, G.H., Lee, J.-W., 2009. Application of gamma irradiation for the enhanced physiological properties of polysaccharides from seaweeds. Appl. Radiat. Isot. 67, 1277–1281.
Fthenakis, V.M., 2001. Multilayer protection analysis for photovoltaic manufacturing facilities. Process Saf. Prog. 20, 87–94.
Gao, H., Zhang, H., Luo, S., Wang, H., 2012. Elementary study on encapsulation reliability of radioisotope battery prototype based on 63 Ni Radio-Voltaic effect. At. Energy Sci. Technol. 46, 375–379.
Guo, X., Liu, Y., Xu, Z., Jin, Z., Liu, K., Yuan, Z., Gong, P., Tang, X., 2018. Multi-level radioisotope batteries based on 60Co γ source and Radio-voltaic/Radio-photovoltaic dual effects. Sensors Actuators A Phys 275, 119–128.
Guo, X., Tang, X., Liu, Y., Jin, Z., Yuan, Z., Xu, Z., Peng, C., Wang, H., 2019. Enhanced novel dual effect isotope batteries: optimization of material and structure. Int. J. Energy Res. 43 (12), 6389–6395.
Hine, G.J., Brownell, G.L., 2013. Radiation Dosimetry. Elsevier.
Hu, G., Hu, H., Yang, Q., Yu, B., Sun, W., 2020. Study on the design and experimental verification of multilayer radiation shield against mixed neutrons and γ-rays. Nucl. Eng. Technol. 52, 178–184.
Huang, S.-K., Hsieh, L.-L., Chen, C.-C., Lee, P.-H., Hsieh, B.-T., 2009. A study on radiation technological degradation of organic chloride wastewater—exemplified by TCE and PCE. Appl. Radiat. Isot. 67, 1493–1498.
Huang, H.-Q., Yang, X.-F., Ding, W.-C., Fang, F., 2017. Estimation method for parameters of overlapping nuclear pulse signal. Nucl. Sci. Tech. 28, 12.
Kellett, M.A., Bersillon, O., 2017. The Decay Data Evaluation Project (DDEP) and the JEFF-3.3 radioactive decay data library: combining international collaborative efforts on evaluated decay data. In: EPJ Web of Conferences. EDP Sciences, p. 2009.
Kim, K.-T., Kim, J.-H., Han, M.-J., Heo, Y.-J., Ahn, K.-J., Park, S.-K., 2017. The study on design of semiconductor detector for checking the position of a radioactive source in an NDT. J. Korean Soc. Radiol. 11, 171–175.
Leo, W.R., 1994. Signal Transmission. Springer Berlin Heidelberg.
Li, X.-Y., Lu, J.-B., Zheng, R.-Z., Wang, Y., Xu, X., Liu, Y.-M., He, R., 2020. Comparison of time-related electrical properties of PN junctions and Schottky diodes for ZnO-based betavoltaic batteries. Nucl. Sci. Tech. 31, 18.
Mohammed, S.D., Majeed, W.Z., Naji, N.B., Fawzi, N.M., 2017. Investigating the influence of gamma ray energies and steel fiber on attenuation properties of reactive powder concrete. Nucl. Sci. Tech. 28, 153.

M'Garrech, S., Ncib, F., 2009. Colorimetric study of effect of gamma-radiation on the color of cotton fabric colored by "henna" dye. Appl. Radiat. Isot. 67, 2003–2006.
Nelson, J., 2003. The Physics of Solar Cells. World Scientific Publishing Company.
Schöppner, M., Plastino, W., Povinec, P.P., Wotawa, G., Bella, F., Budano, A., De Vincenzi, M., Ruggieri, F., 2012. Estimation of the time-dependent radioactive source-term from the Fukushima nuclear power plant accident using atmospheric transport modelling. J. Environ. Radioact. 114, 10–14.
Sellin, P.J., Vaitkus, J., n.d. New materials for radiation hard semiconductor dectectors 557, 479–489.
Shagufta, N.A.Z., 2007. Aqueous solution of basic fuchsin as food irradiation dosimeter. Nucl. Sci. Tech. 18, 141–144.
Shu, D.-Y., Geng, C.-R., Tang, X.-B., Gong, C.-H., Shao, W.-C., Ai, Y., 2018. Analysis on the emission and potential application of Cherenkov radiation in boron neutron capture therapy: a Monte Carlo simulation study. Appl. Radiat. Isot. 137, 219–224.
Tang, X., Liu, Y., Ding, D., Chen, D., 2012. Optimization design of GaN betavoltaic microbattery. Sci. China Technol. Sci. 55, 659–664.
Wirtenson, G.R., White, R.H., 1997. Long-term bleaching of optical glasses darkened by Co60 ionizing radiation. In: Photonics for Space Environments V. International Society for Optics and Photonics, pp. 53–59.
Yusof, N., Mod Ali, N., Hilmy, N., 2007. Types of radiation and irradiation facilities for sterilization of tissue grafts. Radiat. Tissue bank. Basic sci. Clin. Appl. Irradiat. Tissue allografts. World Sci. Publ. Singapore 109–119.
Zhang, R., Gong, P., Tang, X., Wang, P., Zhou, C., Zhu, X., Gao, L., Liang, D., Wang, Z., 2019. Reconstruction method for gamma-ray coded-aperture imaging based on convolutional neural network. Nucl. Instruments Methods Phys. Res. Sect. A Accel. Spectrometers, Detect. Assoc. Equip.